ME 4042

# Zipline P2 Delivery Droid Modelling and Analysis

Team Members: Daanish Islam, Andrew Stamper, Keenan Vaughn

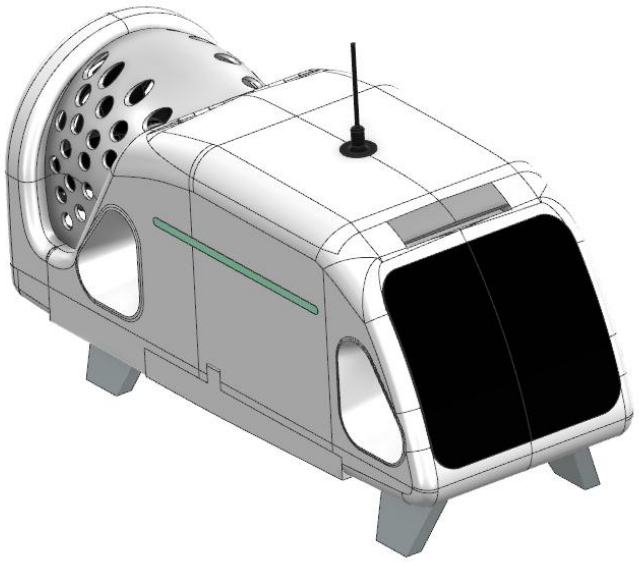

5-4-2026

# Contents

# Introduction

**FIGURE 1: ZIPLINE P2 DRONE DELIVERY SYSTEM (ARROW POINTING TO "DROID")**

The Zipline P2 drone delivery system is meant for accurate door-step deliveries in urban settings. The bigger drone hovers at 300 feet above a house while the smaller drone (the “droid”) drops down to the house’s doorstep to deliver. Zipline claims “dinner-plate” levels of accuracy with the placement of the package. To do this, the droid has 3 different motors / propellers (props) that help orient itself. These motors not only need to be capable of providing enough power to position the drone, but to do so while also counteracting loads due to wind.

Accurate deliveries are not possible without the motors / props in the droid, meaning they (and the components that support them) are essential to the overall functioning of the drone delivery system and need to be carefully designed to ensure they meet the system’s key performance specifications (specs). The goal of our project is to accurately model the droid and understand the engineering decisions made to achieve these specs.

## Objectives

The objectives of the project are:

- Develop components that accurately represent the Zipline P2 droid
    - This is so the forces / stresses acting on the droid can be accurately modeled
- Perform computational fluid dynamics (CFD) analysis on the main body to get the total wind load on the droid
    - This is so a spec for the necessary motor thrust to cancel out wind load can be calculated
- Perform stress analysis on the motor mounts to ensure they do not break during max propeller thrust
    - Parametrize this analysis as a function of motor mount thickness and material to inform the design of the motor mount

# Geometric Modeling

This section provides a brief overview of the function of each part within the final assembly and explains how each part was modeled / assembled. Parts are organized into their respective sub-assemblies.

## Main Body

The main body is the essential base to which all the other subassemblies of the delivery droid will be attached to. Not only does it need to match the likeness to the current design of the droid, but it also needs to be designed with different compartments and open areas for other subassemblies and parts to seamlessly slot in and mated to without any interferences.

The body was created, starting with importing Raster Images of the drone from all six sides into NX and scaling them to match the known bounding box of the drone. From these images, bounding curves resembling the general shape of the body were created. Because the main body is symmetrical, however, the bounding curves were made for just half of the body. Surfacing techniques such as Through Curves, Through Curve Meshes, and Studio Surfaces were all used to create the sheet body of the half of the main body. From there, the sheet body was mirrored to create the whole main body as a sheet, and then all the surfaces were sewn together to create the solid body. Additionally, to create a smoother surface, the Edge Blend feature was used along as many surface edges as possible.

Following the creation of the smooth body, all that was left was subtracting sections out of the body, as well as adding some extruded features, to facilitate the joining of other parts and subassemblies to the main body. This included subtracting the two areas where the side propeller assemblies get installed using a Sweep subtract, as well as subtracting the back propeller and motor space with just Extrude cuts. The spaces for the light bar parts, the drone feet, and the front screen are also Extrude cut out of the body. The last preparations for the main body included Extrude subtractions for the lid, food/medicine compartment, and bay doors, as well as extruding out hinges to connect to the lid part.

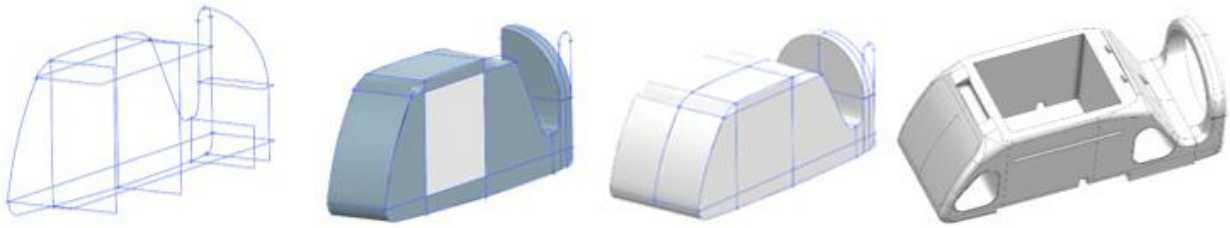

**FIGURE 2: MAIN BODY PROGRESSION**

## Drone Feet

The drone feet were also modeled based off the reference images of the different sides of the drone. To keep assembly down the line as simple as possible, a rectangular extrude was used for the connection point of the feet to a rectangular extrude cut made on the main body. For the complexity of the feet, the Through Curves feature was used to connect the bottom of the rectangular extrude to another rectangle sketch that was decreased in size and offset a good bit to

allow for the feet to be at an angle when looking onto the feet from the front of the drone.

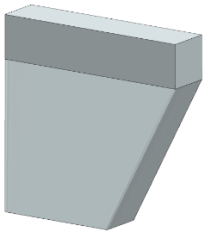

**FIGURE 3: DRONE FEET**

## Front Screen

The front screen was a straightforward part to make, but it required a deeper understanding of a couple of features offered through NX. Starting in the Main Body part file, a 2D sketch of the curved screen box was created in front of the body, and then the sketch was projected onto the contoured front. Then within a new part file, the WAVE Geometry Linker feature was used to create an instance of both the front face and the projected curve of the main body as a reference. From there, I was able to take the projected curve and thicken it to create the final screen to be used in the assembly.

**FIGURE 4: FRONT SCREEN**

## Light Bars

The light bars created are just to represent where on the side of the drone there is a line of LEDs. The geometry of this part was not extremely complex, as it was just a very long rectangle with two semicircles at the end that were extruded. The dimensions of the light bar were also based off the reference images of the side of the drone. Also, since the light bar is typically integrated into the main body to where it is essentially flush with the side panel, the thickness of the light bar was a key dimension to consider, so that it would fit in without interfering or breaking into other extrude cut sections in the body like the food/medicine compartment.

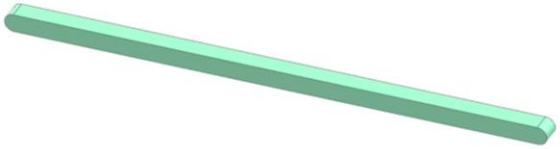

**FIGURE 5: LIGHT BAR**

## Propeller Shroud

The propeller shroud was a very complex part to model. One thing that was difficult about this part was that it required a good amount of linked geometry to base the sketches of the shroud on. Once the sketch of the side profile of the shroud was made, it was extruded to the centerline of the drone, and then it was mirrored to complete the entire shroud off symmetry. The extrusions were then united and shelled so that rather than a solid body filling the entire void space where the shroud goes, it was a shelled surface that could cover the propeller assembly entirely. Finally, to represent the patterned venting on the shroud that the typical droid model has, the hole feature with a patterned circle layout was used.

**FIGURE 6: PROPELLER SHROUD**

## Lid

The lid was an interesting part to create, because it involved taking an already existing part of a solid body, the top part of the main body, and bringing it into a new part file for modifications and easier assembly opportunities. The need to create the lid off the main body came from the desire to have the lid keep the same curvature as that of the body. So, the main body geometry was linked into a new part file, and an Extrude intersection was used to take just the section of the top of the main body that was wanted for the lid. An extrude cut was then performed to make room for the lid handle and tether connection, and extrusions for a part of a hinge were created to make connection to the main body feasible.

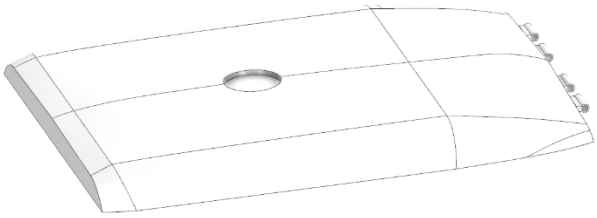

**FIGURE 7: LID**

## Lid Handle

The lid handle was created because without it there would be no easy way to rotate the lid due to the seamless transition from the lid into the main body without it. The lid handle was just created as an extrusion off the linked geometry of the made lid part. Again, the lid was made in the extrude

cut area of the lid, and it was designed so that there was a clear space for a hand to reach in and lift the lid.

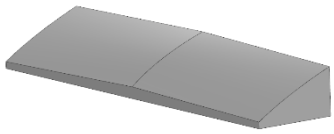

**FIGURE 8: LID HANDLE**

## Lid Hinge Pins

The lid hinge pins were a very straight forward and simple part to make. All it required was an extrusion of a circle to create a cylinder that had the same dimensions of the holes created on both hinge extrusions to seamlessly be mated later down the line and hold the lid connected to the main body.

**FIGURE 9: LID HINGE PIN**

## Tether Connection

The tether connection is what connects the droid to the tether from the main drone. The tether is glued into the tether connection, and the tether connection is glued onto the main body lid. The tether connection is comprised of 3 circular extrudes, with an edge blend between each.

**FIGURE 10: TETHER CONNECTION**

# Side Motor System

The side motor system is responsible for counteracting wind loads and positioning the droid during delivery. It is comprised of a motor, a propeller, and a mounting plate that attaches the motor to the main body. The side motor system was based off current modern drone motors / propellers (see figure below).


**FIGURE 11: EXAMPLE MODERN DRONE MOTOR (EMAX ECO II 2807)**

## Side Motor Base

The side motor base is what connects the stator to the side motor mount. The stator is welded onto the base, and the base is screwed onto the mount. This part is simple, comprised of only 1 sketch / extrude.

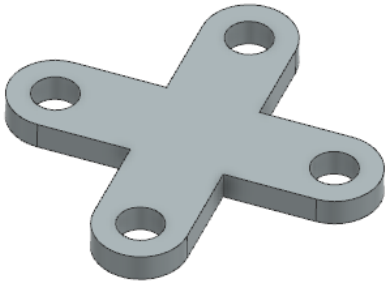

**FIGURE 12: SIDE MOTOR BASE**

## Side Motor Stator

The side motor stator is what passes electric current into the surrounding coils to generate a magnetic field for motor rotation. The coils are welded onto the stator, and the stator is welded onto the motor base. This part is comprised of 2 circular extrudes.

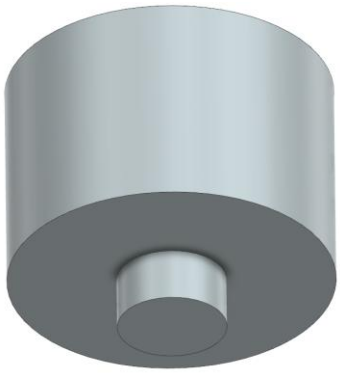

**FIGURE 13: SIDE MOTOR STATOR**

## Side Motor Coil

The side motor coils are what turn electric current into a magnetic field to spin the rotor. The coils are welded onto the stator and do not come in contact with the rotor. This part was modeled by first creating one coil "winding" comprised of an extruded oval and edge blend. Then, the resulting body was patterned 10 times to create the final coil.

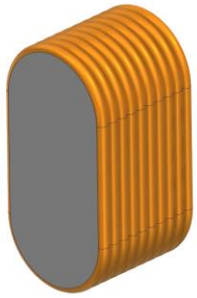

**FIGURE 14: SIDE MOTOR COIL**

## Side Motor Rotor

The side motor rotor spins the propeller to generate thrust. The rotor has permanent magnets glued onto the inner cylindrical surface (not modeled) that respond to the magnetic field generated by the coils. This part was created by first sketching the cross-sectional view of the rotor, then rotating / sweeping that sketch around the central axis of the rotor. The threaded connection for the propeller on top was created by using the NX thread feature on a circular extrude. The lightweight / cooling cutouts on the top of the rotor were created using an extrude cut.

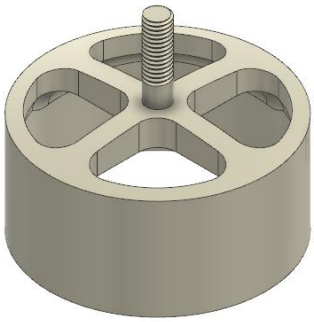

**FIGURE 15: SIDE MOTOR ROTOR**

## Side Motor Propeller

The propeller is what generates thrust to counteract wind forces and position the drone. The propeller is threaded onto the stator. The center of the propeller is a simple circular extrude and an edge blend. The blades of the propeller were created using the "swept" feature: 4 parallel planes along the length of the blade were created, then the cross-sectional profile of the blade at the location on the blade of the respective plane was sketched on each plane. Then, using a straight line that passed through the center of each sketch as a guide curve, the swept feature was applied (shown in the figure below).

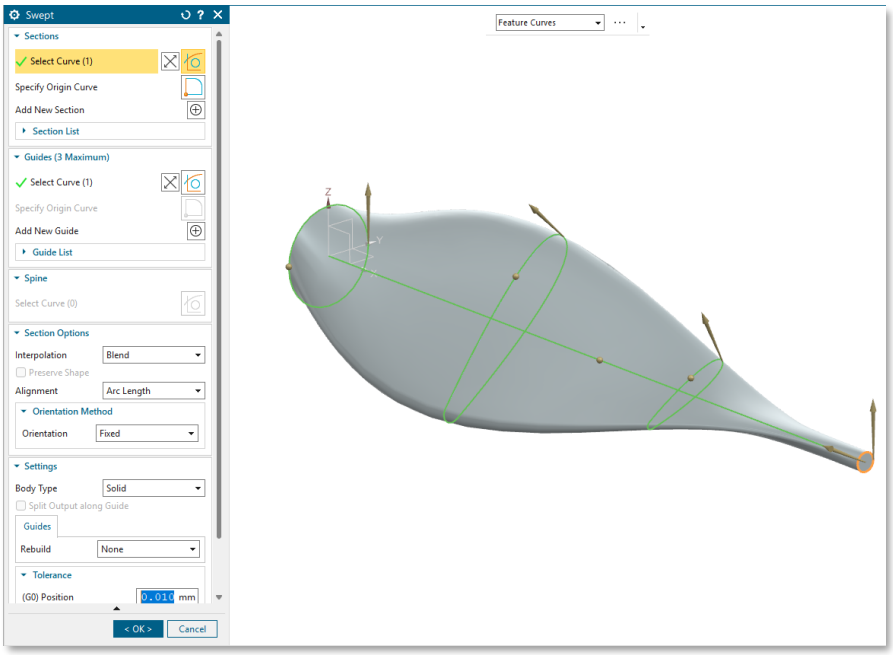


**FIGURE 16: PROPELLER MODELLING SCREENSHOT**

**FIGURE 17: SIDE MOTOR PROPELLER**

## Side Motor Mount

The side motor mount is what connects the motor to the main body. The motor base is screwed onto the motor mount, and the motor mount is press-fit into the main body. This part is comprised of one extrude and an external edge blend.

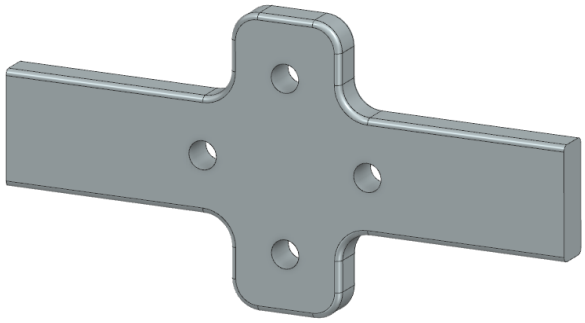

**FIGURE 18: SIDE MOTOR MOUNT**

### Side Motor Sub-assembly

The complete side motor sub-assembly is shown below. First the motor was created by circular-patterning the coils onto the stator. Then, the stator and coils were mated coincident to the motor base. A concentric mate was made between the propeller, rotor, and stator. The whole motor sub-assembly was then mated coincident to the motor mount, with concentric mates at the bolt holes to ensure they were lined up correctly.

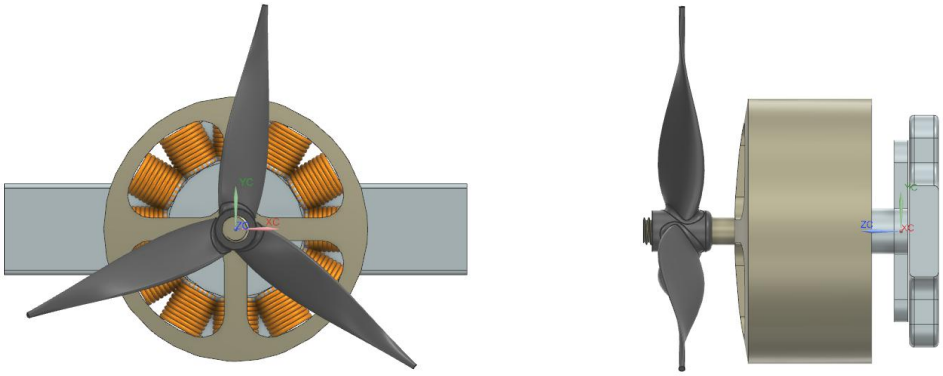

**FIGURE 19: SIDE MOTOR SUB-ASSEMBLY**

## Bay Door Mechanism

### Bay Door Panels

The bay door panels form the underside hatch of the droid and open to release the delivery package. Rather than being modeled as independent parts, the door panels were created as cutouts from the main body solid. A rectangular profile was sketched on the underside of the main body and extruded as a subtraction, generating the bay opening and simultaneously defining the panel geometry from the removed material. This approach ensured geometric consistency between the panels and the body opening, eliminating fit issues during assembly. Each panel was then shelled to a uniform wall thickness. The outer face of each panel follows the curved contour of the droid's underbelly, transitioning from a flat bottom to a gentle upward curve at the lateral edges to blend with the main body profile.

The rack interface was modeled directly on each panel. A rectangular rack bar profile was sketched on the inner surface of each door panel and extruded inward, forming the rack as an integral feature of the door rather than a separate mating part. Gear teeth were added to the exposed top face of this rack extrusion using a patterned trapezoidal cut feature, as described further in Section 3.2. The two panels are mirror images of each other about the longitudinal symmetry plane of the body.

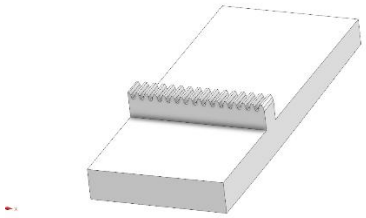

**FIGURE 20: BAY DOOR PANELS**

## Rack and Pinion

The bay door mechanism translates rotational motor output into simultaneous linear motion of both door panels. It consists of six parts: a motor, motor mounting plate, pinion gear, left rack, right rack, and a gasket seal between the motor face and mounting plate. The racks are integral to the door panels as described in Section 3.1 and are not separate floating components, each rack is permanently attached to its respective door panel and slides with it.

The motor housing was modeled as a rectangular extrusion with rounded corners. Longitudinal heat sink fins were added to the outer faces using a patterned rectangular extrude feature. A circular boss was extruded from the front face to represent the motor shaft collar, and a cylindrical shaft was extruded from its center to interface with the pinion.

The mounting plate was modeled as a flat rectangular extrusion with four counterbore holes at the corners for bolted attachment to the main body, and a central circular cutout matching the motor shaft collar diameter.

The pinion gear was modeled as a cylinder of the appropriate pitch radius. Gear teeth were created by extruding a single trapezoidal tooth profile radially outward from the cylinder face, then using the Pattern Feature command with a circular array to distribute teeth evenly around the full circumference. A central through-hole was added to receive the motor shaft.

Since the racks are integrated into the door panels, no separate rack parts were modeled. The tooth profiles on the panel-mounted racks were created using the same trapezoidal sketch as the pinion teeth, applied as a patterned extrude cut along the inner top face of each door's rack extrusion, ensuring proper tooth geometry for mesh engagement with the pinion.

The gasket was modeled as a thin flat extrusion matching the motor face profile with a central circular cutout.

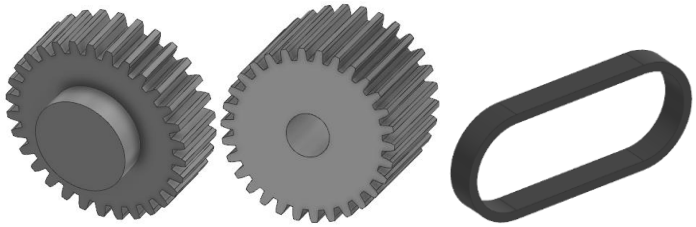

**FIGURE 21: GEAR, PINION AND BELT**

## Bay Door Mechanism Sub-assembly

The bay door mechanism was assembled as a standalone sub-assembly. The motor was first fixed at the origin of the sub-assembly. The mounting plate was constrained to the motor rear face using a touch constraint on their mating faces and a concentric constraint aligning the central shaft hole to the motor shaft axis. The pinion was constrained concentrically to the motor shaft using an inferred axis command and a touch constraint locating it axially against the motor face collar. A revolute joint was defined at the shaft axis to represent motor rotation.

The door panels, with their integral rack features, were then positioned symmetrically on either side of the pinion such that the rack teeth mesh with the pinion teeth on the left and right sides respectively. Each door panel was given a translational joint along its sliding axis, parallel to the body's lateral direction, and a rack-and-pinion motion coupling was defined between the pinion revolute joint and each panel's translational joint. This coupling enforces equal and opposite linear displacement of both panels for a given pinion rotation. When the motor drives the pinion, both door panels slide simultaneously outward in opposite directions along their constrained axes, exposing the bay opening. Reversing motor direction retracts both panels back to the closed position. Because the racks are part of the door panels themselves, the entire door and rack assembly translates as a single rigid body with no secondary joints required.

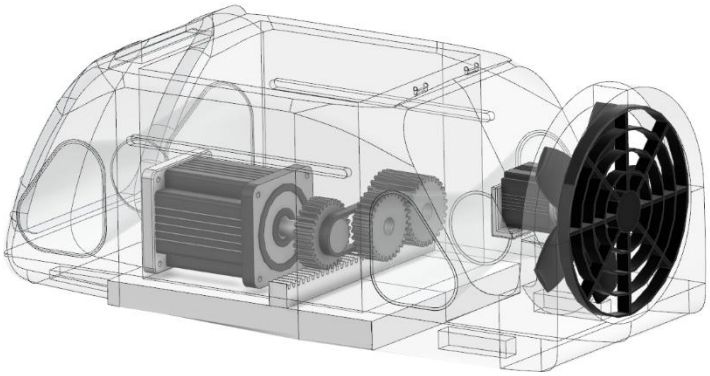

**FIGURE 22: BAY DOOR MECHANISM SUB-ASSEMBLY**

# Main Propeller

## Motor and mount

The back motor assembly generates the primary thrust for the droid's orientation control. It consists of four parts: a motor housing, propeller, propeller cover, and mounting bracket.

The motor housing geometry mirrors that described in Section 3.2, with heat sink fins patterned on the outer faces and a shaft extrusion on the front face.

The mounting bracket was modeled as an L-shaped extrusion. The vertical face contains two through-holes for attachment to the main body, and the horizontal shelf contains a circular cutout and bolt pattern matching the motor rear face. Edge blends were applied at the internal corner of the L-profile to reduce stress concentration.

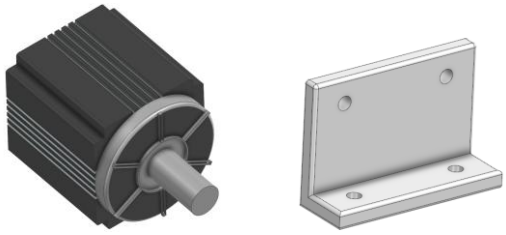

**FIGURE 23: MOTOR AND MOUNT**

## Propeller

The propeller blades present the greatest modeling complexity in the assembly. Rather than simple planar extrusions, each blade was defined using cross-sectional sketches on a series of offset datum planes along the blade span. Each sketch captured the varying chord and twist angle of the airfoil profile. A Through-Curves feature was then used to loft a smooth surface through all cross-sectional sketches, producing a twisted blade geometry. This process was repeated for a single blade, which was then patterned in a circular array of five instances around the hub axis. The hub itself was modeled as a central cylindrical boss with a tapered bore to receive the motor shaft, combined with a short cylindrical collar using a Unite operation.

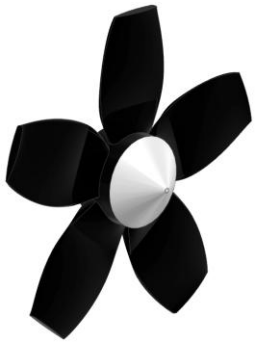

**FIGURE 24: MAIN PROPELLER**

## Propeller Cover

The propeller cover is a circular guard that protects the spinning blades and directs airflow. It was modeled as a flat annular ring, a circular extrude with a concentric circular subtraction,

representing the outer rim. Radial structural bars were added by extruding rectangular profiles from a central hub ring outward to the outer rim, patterned in a circular array. The resulting geometry replicates the cage-like guard visible in the reference images.

**FIGURE 25: PROPELLER COVER**

### Main Propeller Sub-assembly

The propeller assembly was built by first fixing the mounting bracket, then constraining the motor to the bracket shelf using touch and concentric axis commands. The propeller hub was constrained concentrically to the motor shaft with a touch constraint locating it against the shaft collar. A revolute joint was defined at the shaft axis to represent spinning motion. The propeller cover was constrained concentrically to the hub axis and fixed axially to the motor face using a distance constraint.

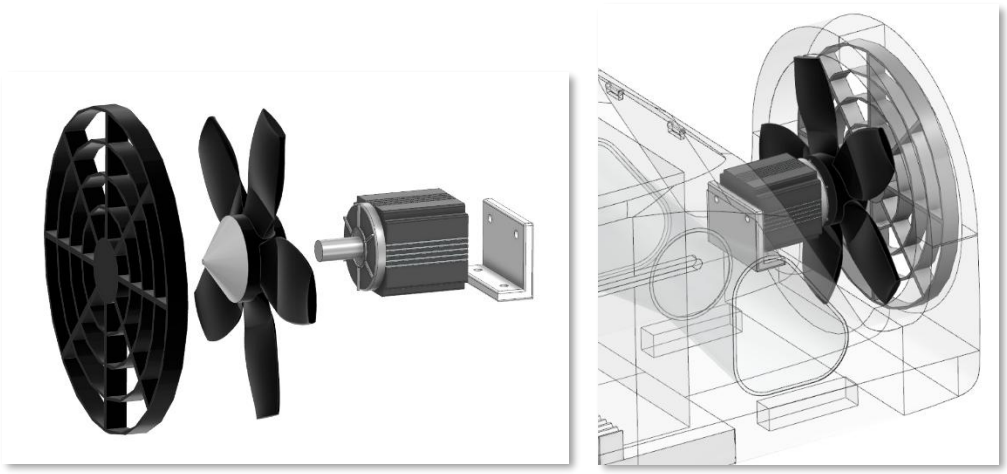

**FIGURE 26: MAIN PROPELLER SUB-ASSEMBLY**

## Assembly

With all the required parts modeled and subassemblies put together, it was time to put together the final assembly. While there were 26 unique parts, 60 total parts were used for the final assembly. The assembling process started with the base as the main body. One by one, the other subassemblies were mated and installed into the body. First the bay door mechanism was added, then the back propeller subassembly, followed by the side propellers, and the lid mechanism. After all of the subassemblies were added, all of the standalone parts such as the feet, light bar, front

screen, propeller shroud, and tether connection were added as finishing touches to the final assembly model.

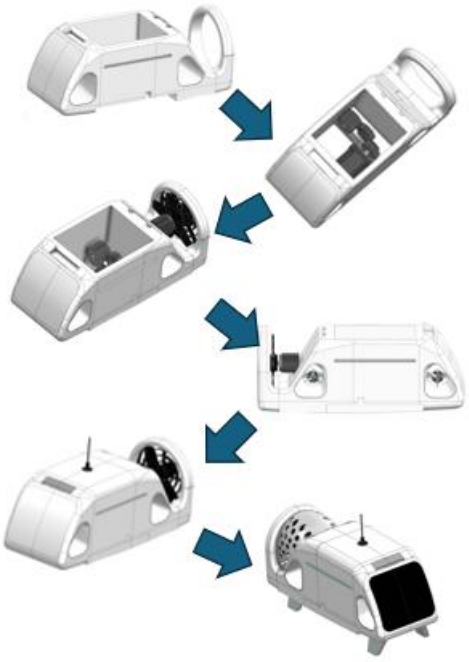

**FIGURE 27: ASSEMBLY FLOW**

There was a good amount of complexity that came from the assembly. In terms of mating all individual parts and subassemblies together, there were not too many complex features used, as there was just a lot of touch and align commands used to limit most degrees of freedom for parts. There were many subassemblies in our model that required a single rotational degree of freedom to be left free, specifically the propellers and the lid hinges, so that they could spin or open and close freely. The most complex mating command used was the limiting of the angle that the lid could open and close, which was set to a 90-degree range of motion about the hinge axis, to prevent any interferences with the main body.

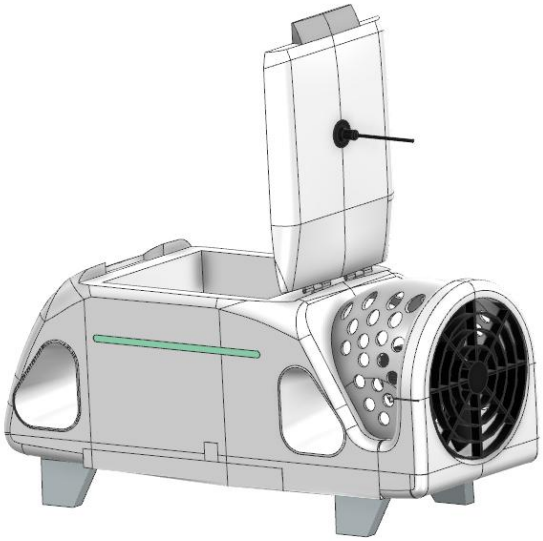

**FIGURE 28: 90-DEGREE LIMITED LID ROTATION ABOUT HINGE**

The primary complexity of the assembly really came before assembly even began, however, as the intentionality during the creation of parts to have perfect interfaces for assembly was really where a lot of work went into. The communication of key dimensions and the use of the subtract command to remove sections of the main body to perfectly slot parts like the tether and small propeller mount into its spot was paramount to the precise assembly that was completed. One additional challenge that was not fully fixed was the integration and imbedding of the bay door opening mechanism, with the limited space of the main body and the inability to fit the very large model of the opening mechanism somewhere other than the space of the food/medicine container.

# Finite Element Analysis (FEA)

This section goes over the FEA conducted on the main body and motor mount that was needed to meet the objectives of the project mentioned in the introduction. Again, those objectives are to:

- Perform CFD analysis on the main body to get the total wind load on the droid
    - This is so a spec for the necessary motor thrust to cancel out wind load can be calculated
- Perform stress analysis on the motor mounts to ensure they do not break during max propeller thrust
    - Parametrize this analysis as a function of motor mount thickness and material to inform the design of the motor mount

## Wind Load on Main Body

### Wind Load Background

As discussed in the introduction, the zipline drone claims “dinner plate accuracy” with deliveries, and it does this by using the propellers on the droid to generate thrust. This thrust not only has to be enough to move the drone but also counteract wind loads.

To spec the motors / props, the max wind load the droid is subject to needs to be calculated. While this can be estimated with a simple "pressure equals force times area," changes in geometry and surface roughness conditions can impact the pressure distribution and resulting wind load on a part under a uniform wind pressure. For a complex geometry such as the main body, these pressure distributions can be difficult to calculate by hand. CFD gives us insight into how changes to the part impact these pressure distributions and can inform design changes.

Below is some terminology that is used in this section:

$$F = total\ wind\ force$$

$$P = wind\ pressure\ (at\ elevation)$$

$$A = approxiamated\ wind\ facing\ area$$

$$\rho = air\ density\ (at\ elevation)$$

$$V = wind\ speed\ (at\ elevation)$$

Below are some statistics of the Zipline P2 drone system and some calculations that were made based on those statistics that guided the CFD analysis.

- Zipline P2 drone flies at 300 ft
    - Highest wind gusts (under normal circumstances, not in hurricane) are around 40mph in an urban setting.
    - Zipline claims their drone can handle gusts of up to 45mph (ref)
- Highest air density is at sea level
    - $\rho = 1.225 \frac{kg}{m^3}$
    - $P = \frac{1}{2}\rho V^2 = 247\ \text{Pa}$
        - $\rho = 1.225 \frac{kg}{m^3}$
        - $V = 45\ mph = 20.1 \frac{m}{s}$

## Wind Load FEA Setup

Below is the general workflow that was taken regarding the CFD:

1. Do a static solve to get an estimate on the wind load using a uniform pressure distribution (this is analogous to F = P*A)
2. Run CFD to see and understand how air flows around the body and get relative pressure map
3. Apply pressure mapping from CFD to a static solver to get the resulting total wind force.
    - Great guide on how to do this: https://www.mayahtt.com/blog/map-flow-forces-structural-analysis-simcenter/

For setting up the simple static solve the main body part was split in half and a fixed constraint was applied at the mid plane. Then, a uniform 247 Pa pressure was applied to all “wind-facing” surfaces of the model. These surfaces were selected using the orientation that the side panels of the main body are completely perpendicular to the direction of the wind). This orientation was selected as it is the worst loading condition for the droid – the side propellers are much weaker than the back propeller. The solver used for this test was Simcenter Nastran, SOL 101 Linear Statics. A screenshot of the static FEA setup is shown below. A CTET 10 mesh with 15mm element size was used.

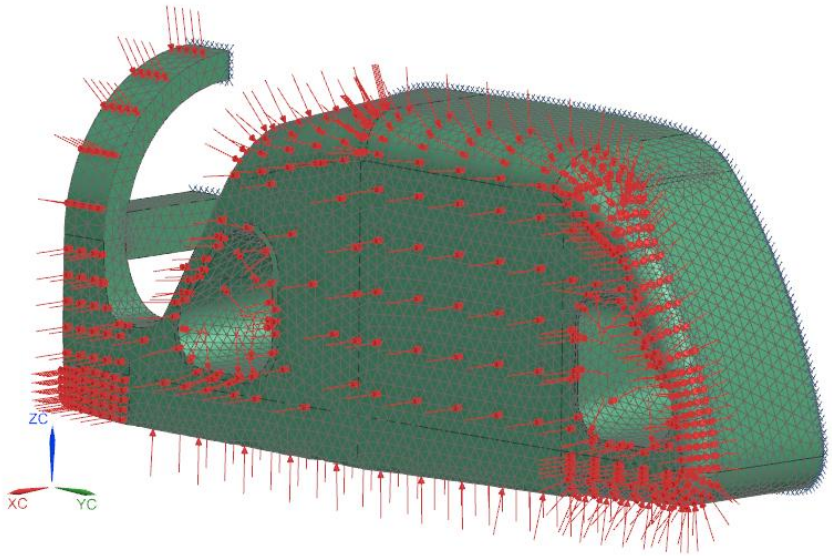


**FIGURE 29: STATIC WIND LOAD FEA SETUP**

The setup for the CFD is quite different compared to that of the static solve. Instead of using the main body part for analysis, volume of air around the main body needs to be created for analysis. This was done by extruding a rectangle around the main body then using the subtract feature with the main body as the tool. This was done twice, once for a smaller volume and once for a larger volume. The smaller volume had a smaller mesh size applied (10mm) to capture the complex behavior of the air close to the main body and get a more accurate value for wind load, and a larger mesh size (100mm) was applied to the larger volume to speed up the time it took for solving the CFD analysis. A “glue” mesh mating condition was applied between these two volumes. CTET10 was used for both tests. Within the .sim file, a 247 Pa flow boundary condition was added at the inlet of the air volume, and an “opening” flow boundary condition was added at the outlet of the air volume. The solver used was Simcenter 3D Flow.

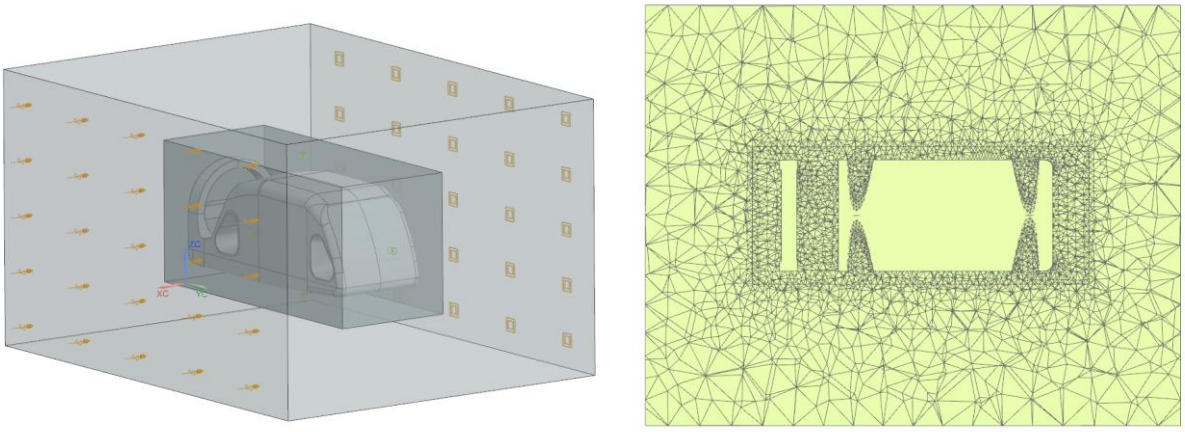

**FIGURE 30: WIND LOAD CFD SETUP**

## Wind Load FEA Results

A table with the results from the simple static FEA and the CFD can be seen below, as well as figures that show the results files from each test. The results are the total summed forces in the x direction (the direction of wind blowing, also the direction that motor thrust is in).

For both tests, the results should be compared to the predicted combined max thrust of the side motors, which is about 10 newtons. This value is a conservative estimate based off common 4-inch drone propellers, which usually have a max thrust of around 500g each.

For both tests the results show that the droid, at least with its current motors / props, cannot position itself in sustained 45 mph winds. While this is an unlikely scenario (as 45 mph winds are only really seen in "gusts," which are usually under 10 seconds long in duration) it does show a weakness of the current system configuration.

When comparing the two tests, it can be observed that the total wind load from the CFD test (114.48 N) is much higher than the static test (67.7 N). This is because the effects of negative pressure cause the 247 Pa wind pressure to act not only on the wind-facing faces of the droid, but also large portions of the non-wind-facing faces of the droid.

**TABLE 1: WIND LOAD FEA RESULTS**

| Result | Value |
|---|---|
| Total wind load (static) | 67.7 N |
| Total wind load (CFD) | 114.48 N |
| Motor max thrust (conservative) | 1000g ≈ 10 N |

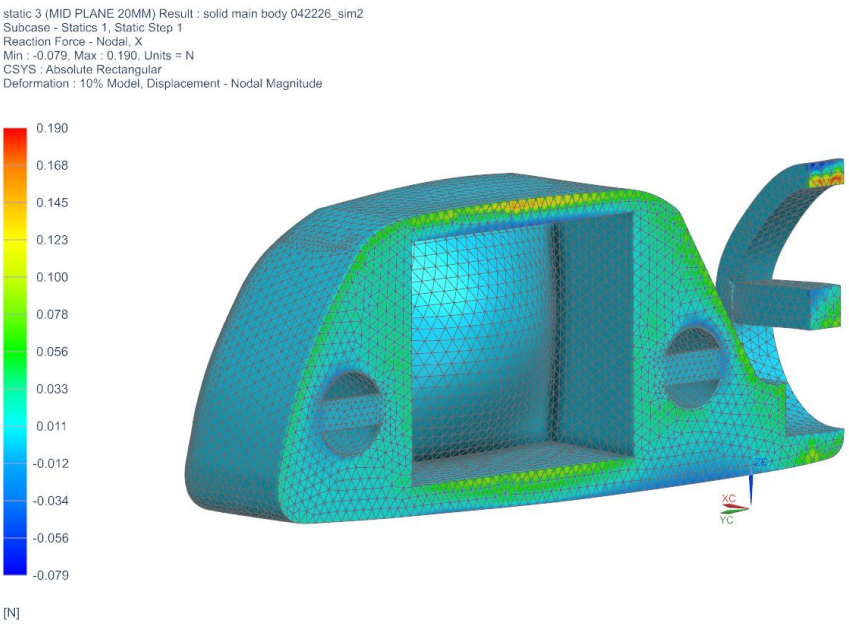


**FIGURE 31: X REACTION FORCE RESULTS, SIMPLE STATIC SOLVE**

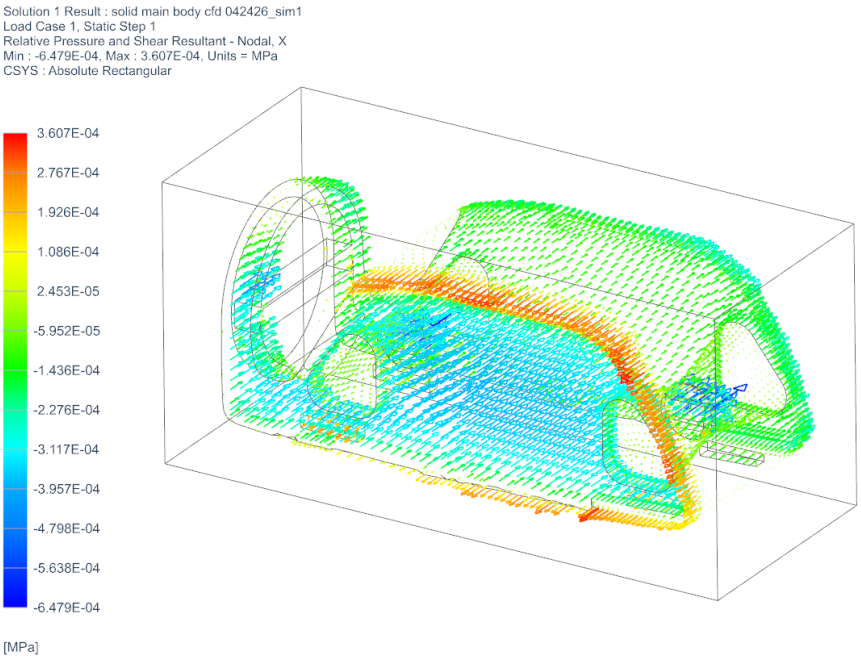


**FIGURE 32: X RELATIVE PRESSURE AND SHEAR RESULTANT, CFD**

# Motor Mount Max Stress

## Motor Mount Background

The main motor mount is a cross-shaped bracket that supports the primary propulsion motor. It must support the motor's max thrust without yielding or deflecting in a way that would misalign the motor and compromise thrust direction. A static structural FEA was performed on this component

to assess its integrity under nominal load conditions and to evaluate the sensitivity of the design to material selection and geometry changes.

The max thrust of the motors was estimated conservatively at 500g based on its compact form factor and comparison to similar-class delivery drones, yielding a static gravitational load of approximately 4.9N. The motor mount was modeled with a baseline material of Aluminum 6061 at a thickness of 0.25 inches (6.35mm).

## Motor Mount FEA Setup

The analysis was conducted in Simcenter NX using the Nastran SOL 101 Linear Statics solver. The motor mount geometry was meshed with 3D solid elements using the CTETRA(10) formulation, 10-node quadratic tetrahedra, at a global mesh size of 1mm, with refinement applied locally around the bolt holes and fillet transitions where stress concentrations were expected. Units were set to mm, N, and MPa throughout.

Boundary conditions were applied to replicate the physical mounting configuration. Both arm end faces were fully constrained with fixed supports locking all six degrees of freedom, representing the bolted connection of the mount arms to the main body. This fixed-fixed assumption represents the worst case for bending stress. The 5N load was applied as a uniform pressure in the negative Z direction over the central pocket surface, the face onto which the motor is bolted, with a net application area of approximately 101.6 × 50.8mm. This load direction is perpendicular to the motor mount surface and produces bending in the arm cross-sections, consistent with the gravitational and dynamic loading experienced in operation.

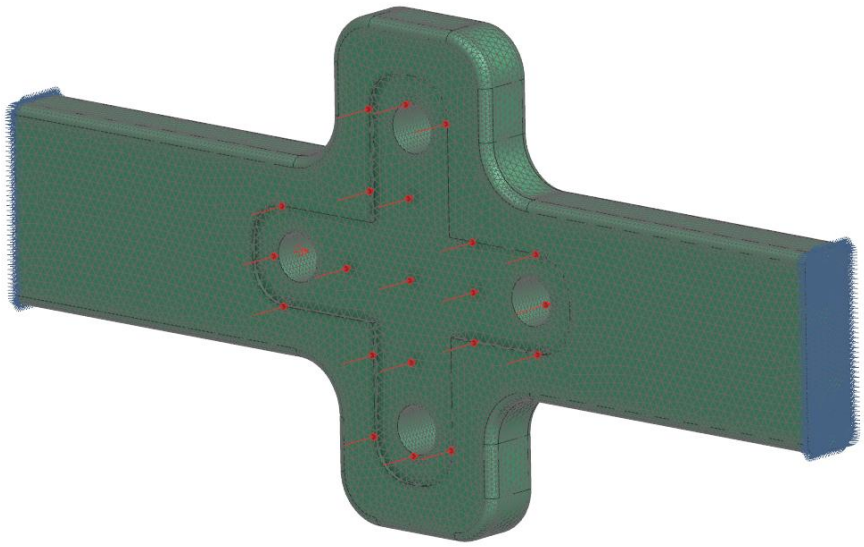

**FIGURE 33: MOTOR MOUNT FEA SETUP**

## Motor Mount FEA Results

The baseline analysis with Aluminum 6061 at 0.25 inch thickness yielded a maximum von Mises stress of 0.589 MPa and a maximum nodal displacement of $9.412\times10^{-4}$ mm. The stress distribution was largely uniform across the arm cross-sections, with slight elevation at the fixed constraint faces and at the fillet transitions between the arms and the central pocket region. This pattern is

consistent with fixed-fixed beam bending theory, in which maximum bending moment occurs at the fixed ends. The elevated stress at the constraint faces is partly a boundary condition artifact, a perfectly fixed wall produces unrealistically steep stress gradients at the constraint interface, and true stress is expected to be somewhat lower at those locations in practice.

The maximum displacement of $9.412\times10^{-4}$ mm is less than one micron, confirming that the part operates entirely within the elastic regime and will experience no measurable deformation under nominal load. Comparing the maximum von Mises stress of 0.589 MPa to the yield strength of Aluminum 6061 (270 MPa) gives a safety factor of approximately 458, indicating that the motor mount is substantially over-designed for this load case. The deformation shown in the contour plots is displayed at 10% model scale for visualization purposes; actual deformation is negligible.

**TABLE 2: MOTOR MOUNT FEA RESULTS**

| Result | Value |
|---|---|
| Max von Mises stress | 0.589 MPa |
| Max displacement | $9.412\times10^{-4}$ mm |
| Material yield strength (Al 6061) | 270 MPa |

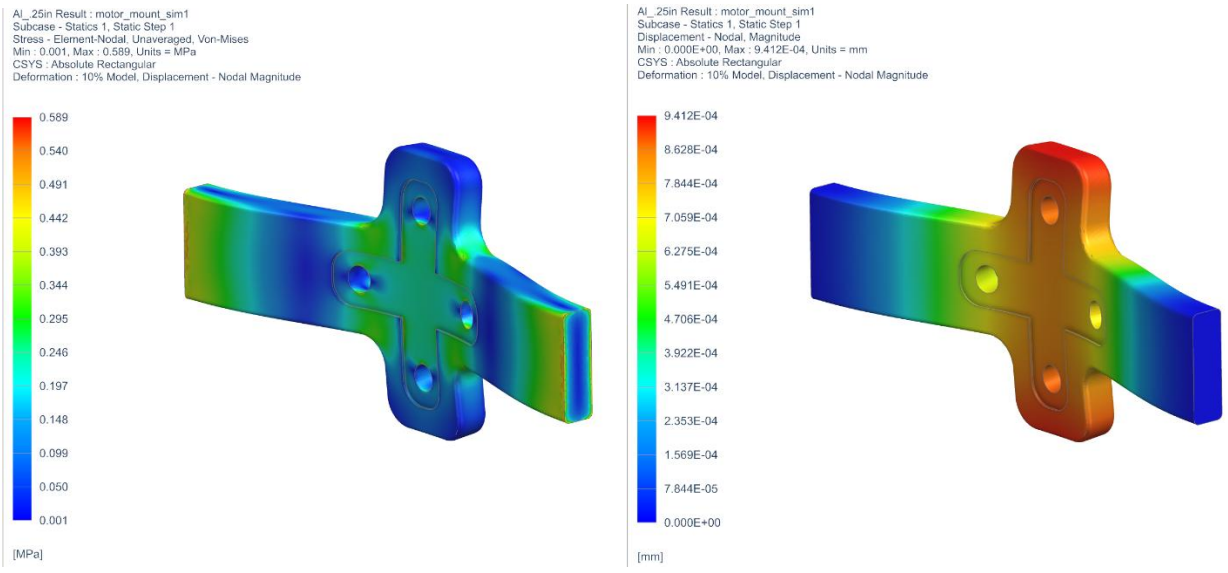


**FIGURE 34: MOTOR MOUNT FEA RESULTS**

## Parametric Study — Material Variation

To evaluate the effect of material selection on structural performance, the FEA was repeated for two additional materials while holding geometry constant at the 0.25 inch baseline thickness. The materials selected were Nylon, representing a lightweight 3D-printed polymer alternative, and Titanium Ti-6Al-4V, representing an aerospace-grade metal. Results for all three materials are summarized below.

The von Mises stress results were nearly identical across all three materials, with values of 0.589 MPa, 0.646 MPa, and 0.590 MPa for Aluminum, Nylon, and Titanium respectively. This result is expected in linear statics: for a given geometry and load, the stress field is determined by equilibrium and is independent of the material's elastic modulus. Stress distribution is therefore geometry-driven, not material-driven.

Displacement, however, varied significantly between materials because it depends directly on stiffness. Nylon, with a Young's modulus of approximately 1,600 MPa, deflected a maximum of 0.0164 mm, roughly 17 times greater than the Aluminum result of $9.412\times10^{-4}$ mm. Titanium, with a modulus of approximately 114,000 MPa, deflected only $5.373\times10^{-4}$ mm, less than Aluminum. Despite these differences in deflection, all three materials passed the yield criterion with large safety factors: approximately 458x for Aluminum, 70x for Nylon, and 1,492x for Titanium. For this application, material selection is therefore driven primarily by weight and manufacturing considerations rather than structural necessity.

**TABLE 3: PARAMETRIC RESULTS VARIATION - MATERIAL**

| Material | Max von Mises (MPa) | Max Displacement (mm) | Yield Strength (MPa) |
|---|---|---|---|
| Aluminum 6061 | 0.589 | $9.412\times10^{-4}$ | 270 |
| Nylon | 0.646 | 0.0164 | 45 |
| Titanium Ti-6Al-4V | 0.590 | $5.373\times10^{-4}$ | 880 |

## Parametric Study — Thickness Variation

To evaluate the effect of arm thickness on structural performance, the FEA was repeated at two additional thicknesses, 0.125 inches (3.175mm) and 0.375 inches (9.525mm), while holding material constant as Aluminum 6061.

Halving the thickness from 0.25 to 0.125 inches increased the maximum von Mises stress from 0.589 MPa to 2.342 MPa, an increase of approximately 4x. This is consistent with beam bending theory, in which bending stress scales with $1/t^2$, so halving the thickness quadruples the stress. Conversely, increasing thickness to 0.375 inches reduced maximum stress to 0.312 MPa. Maximum displacement followed the same trend, decreasing from $9.412\times10^{-4}$ mm to $2.945\times10^{-4}$ mm as thickness increased, reflecting the higher second moment of area resisting bending more effectively.

Even at the minimum tested thickness of 0.125 inches, the safety factor remains 115x, indicating that all three thickness variants are structurally sound under the applied load. From a weight and material optimization standpoint, 0.125 inches is structurally sufficient, but the baseline 0.25 inch design is preferred in practice because it provides greater stiffness that better preserves motor

alignment under dynamic conditions, misalignment of the motor would degrade thrust precision, which is operationally critical for the droid.

**TABLE 4: PARAMETRIC RESULTS VARIATION - THICKNESS**

| Thickness | Max von Mises (MPa) | Max Displacement (mm) |
|---|---|---|
| 0.125 in (3.175mm) | 2.342 | $7.328\times10^{-3}$ |
| 0.25 in (6.35mm) | 0.589 | $9.412\times10^{-4}$ |
| 0.375 in (9.525mm) | 0.312 | $2.945\times10^{-4}$ |

# Hand calculations and Validation

## Wind Load

To verify the FEA setup and results, an approximated wind load was calculated by hand. This calculation is a simple "force equals pressure times area" calculation (see figure below). In this case, the pressure is the calculated 247 Pa pressure that was calculated previously (this represents the air pressure under 45 mph wind gusts). The area is the wind-facing area of the droid, which is the projected side area (shown in figure below).

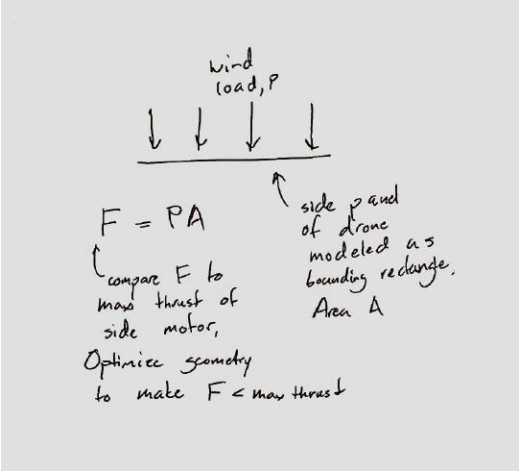


**FIGURE 28: WIND LOAD FEA HAND CALC SETUP**

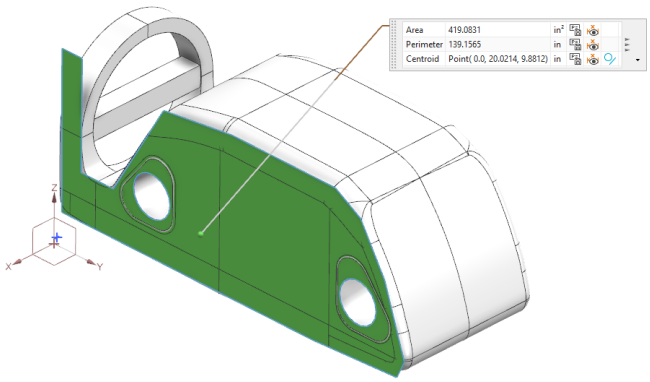


**FIGURE 29: PROJECTED WIND-FACING AREA OF DROID**

The results from the hand calculation are shown below. The resulting wind load was calculated to be 66.7 N. This validates the wind load FEA done previously, as it is just 1 N (less than 2%) off from our static FEA. It's much further away from the 114 N of CFD test, but this makes sense as the hand calculation does not account for the effects of negative pressure / wind load on the non-wind-facing faces.

- $F = PA = 66.7\ N$
  - $A = 420\ in^2 = 0.27\ m^2$
  - $P = \frac{1}{2}\rho V^2 = 247\ \text{Pa}$
    - $\rho = 1.225\ \frac{kg}{m^3}$
    - $V = 45\ mph = 20.1\ \frac{m}{s}$

## Motor Mount

To verify the FEA setup and results, the motor mount was simplified to a fixed-fixed beam under a central point load, consistent with the loading and boundary conditions applied in the simulation. This classical beam model allows an independent estimate of maximum bending stress and deflection for comparison.

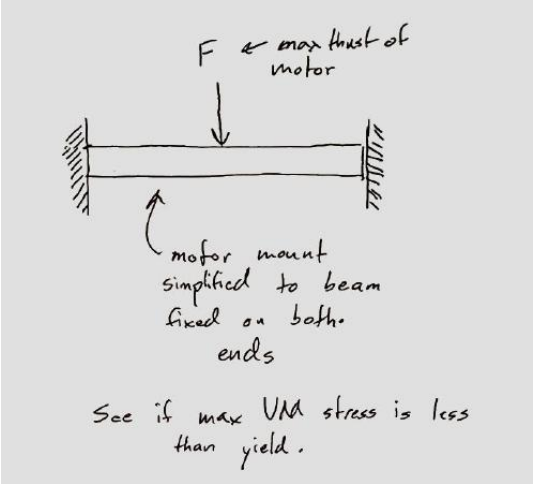


**FIGURE 30: MOTOR MOUNT FEA HAND CALC SETUP**

The beam was defined with the full arm span as its length (L = 101.6mm), the arm width as its cross-section breadth (b = 50.8mm), and the arm thickness as its cross-section height (t = 6.35mm). The material modulus for Aluminum 6061 was taken as E = 69,000 MPa.

For a fixed-fixed beam with a central point load F, the maximum bending moment occurs at the fixed ends and is given by:

$$M = FL/8.$$

Substituting F = 5N and L = 101.6mm gives M = 63.5 N·mm. The second moment of area of the rectangular cross-section is

$$I = bt^3/12 = (50.8 \times 6.35^3)/12 = 1{,}086\ \text{mm}^4$$

The maximum bending stress is then:

$$\sigma = Mc/I$$

Where c = t/2 = 3.175mm, giving:

$$\sigma = (63.5 \times 3.175)/1{,}086 = 0.186\ \text{MPa}.$$

The maximum central deflection for a fixed-fixed beam with a central point load is given by:

$$\delta = FL^3/192EI$$

Substituting the values above gives

$$\delta = (5 \times 101.6^3)/(192 \times 69{,}000 \times 1{,}086) = 3.6 \times 10^{-4}\ \text{mm}$$

Comparing these hand calculation results to the FEA output, the FEA maximum stress of 0.589 MPa is approximately 3x higher than the hand calculation value of 0.186 MPa, and the FEA maximum displacement of $9.412\times10^{-4}$ mm is approximately 2.6x higher than the hand calculation value of $3.6\times10^{-4}$ mm. Both results are the same order of magnitude, confirming that the FEA setup is reasonable and correctly configured.

The discrepancy between the two methods is expected and physically explainable. The hand calculation assumes a prismatic rectangular beam with no material removed, whereas the actual motor mount has a pocket cutout at the center, four bolt holes, and fillet transitions between the arms and the raised center section. These geometric features reduce the effective section modulus at critical locations and introduce local stress concentrations that the hand calculation cannot capture. The FEA, which resolves the full geometry with a fine tetrahedral mesh, correctly predicts higher stress at these locations. The close agreement in order of magnitude validates the FEA boundary conditions and loading, while the quantitative difference is fully accounted for by the geometric complexity ignored in the simplified beam model. Both analyses confirm that the safety factor is very large and the motor mount will not yield under nominal operating load.

**TABLE 5: COMPARISON BETWEEN FEA AND HAND CALC RESULTS**

| | Hand Calc | FEA |
|---|---|---|
| Max stress | 0.186 MPa | 0.589 MPa |
| Max displacement | $3.6\times10^{-4}$ mm | $9.412\times10^{-4}$ mm |

## Summary and Concluding Remarks

Overall, the modeling process of the Zipline P2 droid was very informative and rewarding, as the team was able to complete a final model that looked very close to the real thing, working just off reference images and bounding box dimensions.

With the nature of this project being that each member of the team took on the responsibility of modeling parts that would eventually be assembled and mated to parts that other group members modeled, the importance of communication of key dimensions and changes of parts became a very important takeaway. This understanding became apparent very quickly, as the team wanted to limit the amount of time that got wasted having to redo work because of a lack of communication.

The results from the FEA analysis on both the wind load and the motor mount max stress show that FEA is an effective tool for informing design decisions. The results gathered, which would have taken an extremely long time to calculate by hand, were insightful in showing specific pressure / stress distributions that impacted the proposed specs of the system. However, as with all FEA, it is extremely important to validate the results with hand calculations.

This project was very beneficial to the team, as it opened opportunities for each team member to grow in their understanding of NX and all its modeling capabilities, while also letting them explore the process of performing FEA on models with hand calculations as a verification tool. The ability to learn so much on a project that the team collectively found interesting rather than just a randomly assigned project was refreshing and made this class the amazing learning experience that it was.